Turbulent flow pressure losses in gasoline particulate filters

Aleksandrova, S., Saul, J., Prantoni, M., Medina, H., Garcia-Afonso, O., Bevan, M. & Benjamin, S.

Original citation & hyperlink:
Aleksandrova, S, Saul, J, Prantoni, M, Medina, H, Garcia-Afonso, O, Bevan, M & Benjamin, S 2019, 'Turbulent flow pressure losses in gasoline particulate filters' SAE International Journal of Engines, vol. 12, no. 4, 03-12-04-0030, pp. 455-470.
https://dx.doi.org/10.4271/03-12-04-0030

DOI 10.4271/03-12-04-0030
ESSN 1946-3944

Publisher: SAE International

Turbulent flow pressure losses in gasoline particulate filters

Author, co-author (Do NOT enter this information. It will be pulled from participant tab in MyTechZone)

Affiliation (Do NOT enter this information. It will be pulled from participant tab in MyTechZone)

ABSTRACT

Gasoline Particulate Filter (GPF) technology is the key method of meeting the new regulations for particulate matter emissions from gasoline cars. Computer Aided Engineering is widely used for the design of such systems, thus the development of accurate models for GPFs is crucial. Most existing pressure loss models require experimental calibration of several parameters. These experiments are performed at room temperatures, or on an engine test bench where gas properties cannot be fully controlled. This paper presents pressure loss measurements for clean GPF cores performed with uniform airflow and temperatures up to 680°C. The flow regime in GPF is shown to be different to that in the Diesel Particulate Filters (DPF) due to high flow rates and temperatures. Therefore, most of the existing models are not suitable for design of the new generation of aftertreatment devices. To separate pressure loss contribution from different sources, unplugged filter cores are tested. A new model to describe pressure losses in GPFs is proposed and validated, taking into account turbulent friction losses and pressure variation along the filter channels. It is shown that friction losses are dominant in clean GPFs, thus shorter filters with high cross-section area may need to be considered - at least for the uncoated GPF applications, - which provide high filtration area while maintaining short channel length and lower pressure loss. It is suggested how the developed "0D" model can be implemented in 3 dimensions using the porous medium approach. Thus, collected data and the proposed models will facilitate the development and design of new aftertreatment systems for modern powertrains, especially engines with Gasoline Direct Injection. The method of separating and assessing the pressure losses from different sources gives an insight into properties of several types of flows (laminar flows with contraction/expansion, slip flows, flows with suction/injection), and opens new avenues for investigation of such flows.

INTRODUCTION

One- and zero-dimensional models for pressure losses in Diesel Particulate Filters have been around for a long time. Based on formulation suggested by Bisset [1], several groups have developed and refined parts of the model (e.g. [2]-[7]), which combines losses from different sources as illustrated in Figure 1. Initial studies focused mostly on friction and through wall losses ([2]). Once it was established that inertial losses may play an important role, flow losses due to flow path contraction and expansion, as well as Forccheimer losses have been investigated in more detail ([3], [4]). Dedicated experimental studies demonstrated the good performance of this approach once the unknown model parameters were estimated (e.g. [5], [6], [7]).

More complex formulations have subsequently been developed to account for the soot/ash accumulation, different regimes of soot loading, regeneration, catalyst layer presence, density changes along the channels, transient effects, slip effect etc. Reviews of these and other studies are available ([8],[9]), and a more detailed base model description with relevant references will be given below. Other models exist ([10], [11]), however these are usually much more complex and present little advantage over one-dimensional versions (e.g. [12]).

Since Gasoline Particulate wall-flow filters have the same base geometry as DPFs, they are generally expected to have similar mechanisms governing the flow, and same sources of pressure losses. DPF pressure loss models have recently been used to study GPF geometries (e.g. [13], [14]). However, these studies are based on parameter fitting, and the resulting values of the flow inertial coefficients are not quoted, which suggests that (similarly to many of the DPF studies) higher pressure losses in GPFs may be masked by artificially inflated inertial losses. Another model suggested by Watling et al [15] uses the more fundamental approach for pressure loss calculation, however the model is rather complex and requires numerical solution.

From fluid dynamics point of view, the principal differences between DPF and GPF flow are higher temperatures, smaller channels with thinner walls and different porous wall properties. This results in higher volumetric flow rates, higher flow velocities, and slip effects becoming important for both friction and through wall losses [16]. An estimate of Reynolds numbers inside the filter channels shows that the flow in a GPF may enter turbulent regime. This could even be the case for DPFs as pointed out by Masoudi [17]. Very few experimental studies of flow inside the channels exist (e.g. [18]) and

these are not sufficiently detailed to provide a definitive answer about the presence of flow transition.

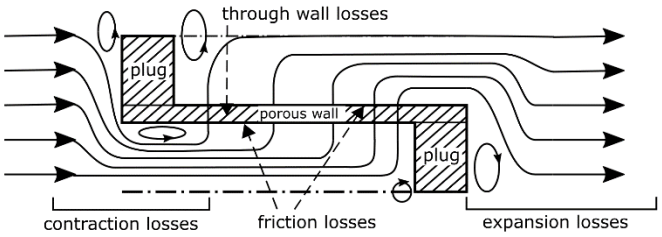

Figure 1 A schematic of pressure loss contributions for a plugged filter: cross-section of half of the inlet and half of the outlet channel.

Experimental and numerical studies of flow transition over a non-permeable porous wall show that one cannot assume that the flow has the same friction and transition properties as flow over a smooth or even rough wall. For example, in laminar flow the friction factor may be reduced due to slip and the reduction of viscous stress near the wall [19]. Transition to turbulence can occur at lower Reynolds numbers (for example, turbulent flow was observed using PIV at Reynolds numbers as low as 1300 [19]). In the turbulent bulk flow regime, Reynolds stress is much higher with permeable walls than it is with rough solid walls [20],[21],[22].

Furthermore, the presence of the wall flow modifies the boundary layer properties considerably. Some early self-similar solutions for uniform suction/injection [23] indicate that friction coefficient increases for injection and decreases for suction, although suction may promote transition to turbulence [24]. The effect on the friction also is very different for different geometries [23], [24]. More recent analytical and numerical studies ([25], [26], [27]) confirm some of these findings while contradict others. An experimental study by Oyewola et al [28] showed that suction may promote relaminarisation in turbulent flows. Some other results suggest that friction in a channel with a porous wall with uniform injection is equivalent to friction in a channel with smooth walls [29].

To sum up, transition properties in a 3-dimensional flow with porous walls and non-uniform wall flow are largely unknown. The stabilising effect of suction has mostly been studied with uniform flow velocity and therefore cannot be directly assumed for filters ([27],[30],[31],[32]).

In this study, pressure losses for several filter cores are measured for a range of flow rates. A brief summary of the existing 0D model based on the work of Bisset [1] is presented with aim to identify uncertainties associated with each pressure loss term. These challenges are then demonstrated by applying the existing models to the experimental results. Finally, several ways to improve the existing model for the high mass flow rate range are suggested and their performance is assessed.

EXPERIMENTAL SETUP

Samples

The testing was performed with 58 mm diameter core samples cut from cordierite monoliths. Six samples were used as specified in Table 1. Cores #2, #3 and #4 also had catalyst coating applied. The monolith channel wall thickness and hydraulic diameter were estimated using the data provided by the manufacturer.

Measurements performed on several randomly selected channels using a Mitutoyo Vision measurement system showed hydraulic diameter values within 5% of the nominal values for all filters. Two cores (#5 and #6) were not plugged and only used for the friction and contraction/expansion loss study.

The open frontal area fraction for each core was calculated as $0.5d_h^2 / a^2$ for plugged cores and d_h^2 / a^2 for unplugged ones (here d_h is the hydraulic diameter of the inlet channel, and a is cell pitch). It is worth noting that there is some degree of uncertainty introduced by area calculations, as due to the circular cross-section of the core samples some channels were only partially open.

Table 1 Core sample properties

	Core #1	Core #2	Core #3	Core #4	Core #5	Core #6
Cell density (cpsi)	300	300	300	300	300	300
Wall thickness (mil)	8	8	8	12	8	8
Length (mm)	125	125	100	125	102	150
Diameter (mm)	58	58	58	58	58	58
Plugged	yes	yes	yes	yes	no	no
Coated	no	yes	yes	yes	no	no
Cell hydraulic diameter (mm)	1.26	1.22	1.22	1.13	1.26	1.26
Wall thickness (mm)	0.203	0.238	0.238	0.327	0.203	0.203
Median pore size (µm)	17.5	10.3	10.3	12.3	17.5	17.5
Median porosity	0.64	0.59	0.59	0.55	0.64	0.64

Hot flow rig

The measurements have been performed on the hot flow rig shown in Figure 2 and Figure 3. Compressed air supplies the two 36 kW Sylvania SureMax heaters (1). A double-skin nozzle (2) with flow straightener plate (3) and extra insulation (not shown in the figure) was designed to mix the hot air from the heaters and provide a uniform flow distribution. An upstream instrumentation section (4) contains 4 pressure tappings located 30 mm upstream of the core spaced equally around the circumference of the pipe, and a thermocouple located 25 mm upstream of the core. The test section (5) holds the core and contains three K-type thermocouples touching the core surface, located at 0.25, 0.5 and 0.75 of the length of the core holder. A downstream instrumentation section (6) contains 4 pressure tappings located 95 mm downstream of the core and spaced equally around the circumference of the pipe. Another thermocouple is located 75 mm downstream of the test section. Although there are extra pressure losses due to friction between the test section and the measurement points, these are negligible compared to the total pressure loss across the filter. An outlet sleeve with an adjustable duct attached (7) directs the hot air into the extractor duct.

The core samples were enclosed in sample holders of appropriate lengths as shown in Figure 4, with 50 mm diameter area available to the flow at both ends.

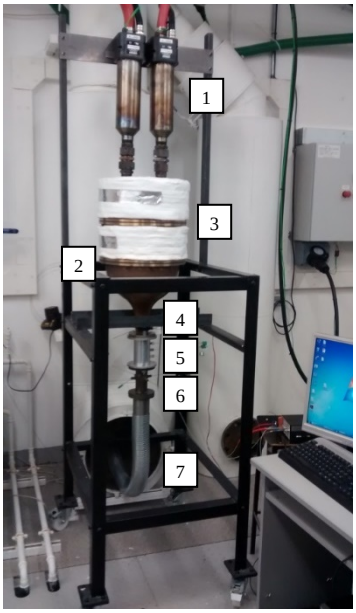

Figure 2 Flow rig

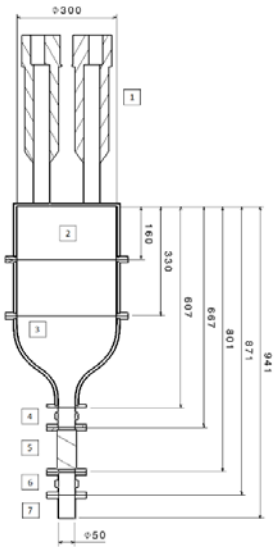

Figure 3 Flow rig dimensions

Figure 4 Core sample holder

Experimental procedure

Pressure measurements upstream and downstream of the test section were performed using digital manometers with accuracy within ±0.25% of the reading. A calibrated Viscous Flow Meter (VFM) was used to set the mass flow rate. Temperatures were measured using K-type thermocouples with an accuracy of ±2.5K.

Measurements were recorded using bespoke LabView interface with LabJack 14 channel data acquisition unit. Continuous logging of all digitally recorded readings was carried out with intervals of approximately 0.5 s. The actual data point recording was triggered manually when the rig was considered in thermal equilibrium, and an average of 10 logged data points was recorded. The variation between these 10 readings was low, within 1% on average. The thermal equilibrium was deemed to be reached when the change in the three core surface temperature readings did not exceed 2K over a period of 5 minutes.

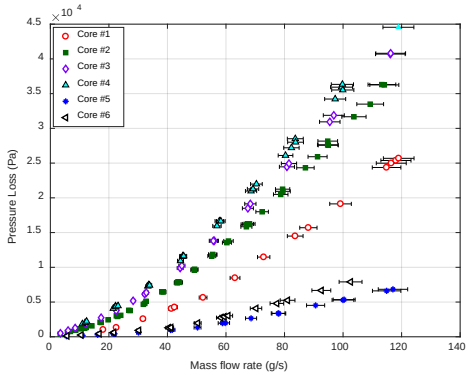

Figure 5 Pressure loss versus mass flow rate (cold flow)

For each temperature point, around 2 hours were needed to reach thermal equilibrium. The testing was started at lower mass flow rates, gradually increasing those until the desired maximum was reached. After each mass flow increment, the temperature of the test section was allowed to stabilise before the reading was taken. Some adjustment of heater temperature was often required to achieve the same temperature in the test section for different mass flow rates. In the first few tests, the mass flow was reduced in the same increments after the maximum flow rate was reached, in order to check repeatability of the results. However, the repeatability was considered very good, and due to time constraints only 3-4 mass flow rate decrements were used in consequent testing to reduce testing time. In addition, some temperature point testing was performed once by increasing the temperature from 20°C to around 680°C, then repeated by decreasing the temperature. Good repeatability of the results was confirmed regardless of whether the temperature was increased from the previous test point or decreased.

Since mass flow rate calculation in a viscous flow meter depends on several variables (absolute airline pressure and temperature, differential pressure across the VFM and calibration line error), the maximum mass flow rate error for the data presented here was 6.5%. The relative error in the back pressure measurements decreases with increase of the measured pressure. It was under 10% for lower pressures (< 2kPa) and below 1% for high pressure values. Pressure measurement errors are not shown in figures for clarity, because the error bars cannot be distinguished from data point markers.

TEST RESULTS

Cold flow

Cold flow test results for all cores are shown in Figure 5. The bare plugged core (Core #1) offers least resistance to the flow compared with the other plugged cores, while the thicker wall coated core 300/12 (Core #4) produces highest pressure losses. Counterintuitively, the shorter (100 mm) coated 300/8 core #3 produces higher back pressure than the longer (125 mm) core #2 of the same specification. This is consistent with other studies [5, 13] and is attributed to the trade-off between friction and through wall losses: the friction losses increase with filter length, while the through wall losses decrease. Pressure losses in unplugged cores #5 and #6 are lower for the same mass flow rates, with the longer core #6 providing more resistance to the flow as expected.

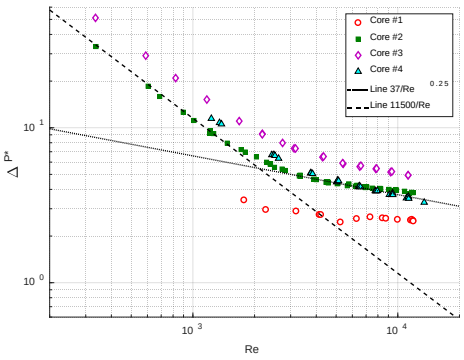

(a)

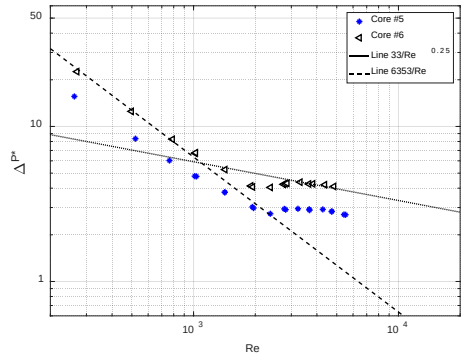

(b)

Figure 6 Non-dimensional pressure loss versus Reynolds number, cold flow: (a) plugged cores #1 - #4; (b) unplugged cores #5 and #6.

The pressure loss in the filter is linked to the volumetric flow rather than the mass flow. Therefore, a characteristic velocity needs to be introduced. Several velocity scales can describe the flow, such as mean superficial velocity, mean velocity at the entrance of the inlet channels, mean velocity inside the filter in all channels, or only inlet channel. Since the highest velocity is achieved near the entrance to the inlet channel in the vena contracta area, the mean velocity at the entrance of the inlet channel has been chosen for flow characterisation. It allows to estimate the highest value of the Reynolds number in the channels, and thus determine the most likely flow regime in the filter channels. The velocity scale is thus defined as

$$U = \frac{\dot{m}}{\rho A_0 \sigma}, \quad (1)$$

where $\dot{m}$ is the mass flow rate in kg/s, ρ (kg/m^3) is air density upstream of the core, A_0 (m^2) is the total cross-section area of the test section and σ is the open area fraction at the front face of the core.

In order to compare flow regimes for different conditions, the flow parameters are non-dimensionalised. The Reynolds number,

$$Re = \frac{U d_h}{\nu}, \quad (2)$$

characterises the importance of inertial effects with respect to viscous ones. Here d_h (m) is the hydraulic diameter of a filter channel and ν is the kinematic viscosity of the air upstream of the core (m^2/s).

Non-dimensional pressure loss is defined as the ratio of total pressure loss to the dynamic pressure:

$$\Delta P^* = \frac{\Delta P}{0.5 \rho U^2}. \quad (3)$$

Plotting the non-dimensional pressure against the Reynolds number shows similar trends for all plugged cores (Figure 6 (a)), although it is clear that other non-dimensional groups play an important role. There is a change in the trend between lower and higher values of the Reynolds number, which will be further examined in the modelling section. For unplugged cores (Figure 6 (b)) the change in trend happens at slightly lower Reynolds numbers and is more pronounced. Two trend lines are added to Figure 6 showing the characteristic slope for laminar (Re^{-1}) and turbulent ($Re^{-0.25}$) friction loss. The factors for these are chosen arbitrarily so that the slope lines are shown next to the test data.

Hot flow

Hot flow testing covered a wide range of temperatures and flow rates. Figure 7 shows the testing results for all four cores. Black symbols represent actual measurement points, while contours show interpolated pressure maps. The results show that for a fixed mass flow rate the pressure loss in the core could nearly triple with the temperature increasing from 20°C to 680°C.

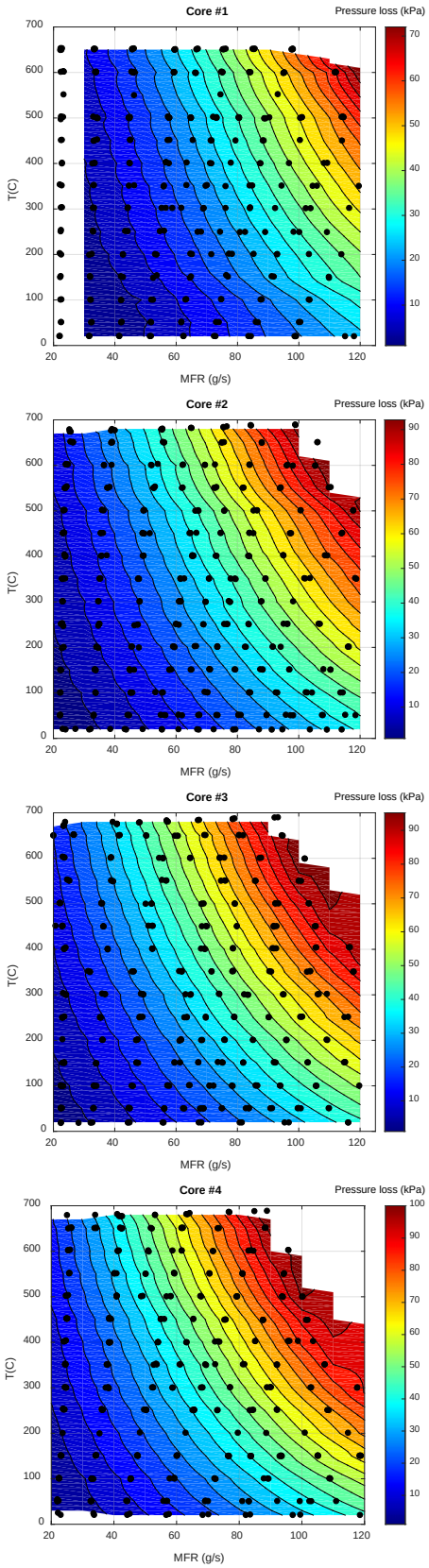

Figure 7 Pressure loss maps for cores 1 - 4. Black symbols show actual measurement points.

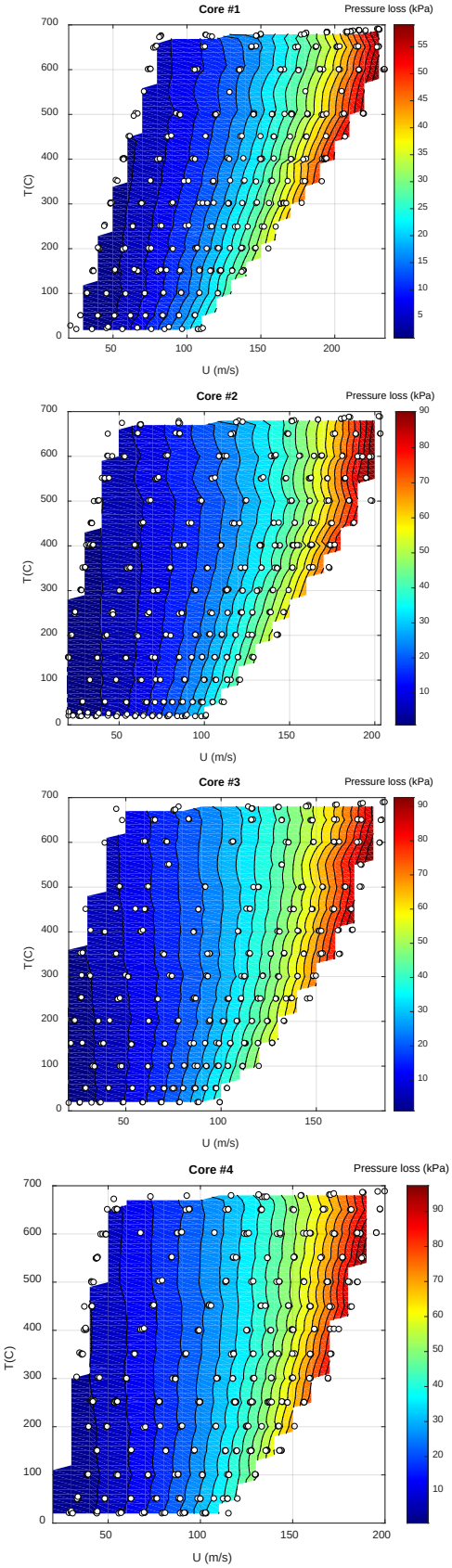

Figure 8 Pressure loss maps for cores 1 - 4. Symbols show actual measurement points.

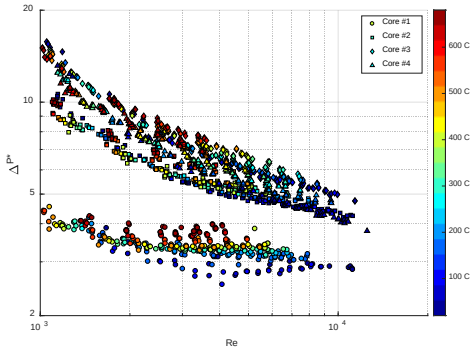

Figure 9 Non-dimensional pressure loss versus Reynolds number. All plugged cores, test results for all mass flow rates and temperatures.

Plotting pressure loss maps using the velocity *U* (Figure 8) shows that for a fixed flow velocity the pressure loss decreases with temperature. This is caused by the gas being more rarefied if the temperature is increased, so that the viscous losses (friction and through wall) are smaller for the same bulk flow velocity.

Non-dimensional pressure plots (Figure 9) show similar trend for all cores with increasing Reynolds number. However, there is still a wide spread between data points for the same values of Reynolds number with different temperatures. This indicates that the flow losses cannot be described solely by Reynolds number, and other non-dimensional groups play an important role.

PRESSURE LOSS: EXISTING 0D MODELS

Pressure loss contributions

Most popular 0-D pressure loss models developed for Diesel Particulate Filters are based on the 1-dimensional model by Bisset [1]. In that work the flow in the filter channels is considered to be one-dimensional with wall stress accounted for in the one-dimensional Navier-Stokes equations. In corresponding 0-dimensional models, the total pressure loss is often expressed as:

$$\Delta P_{total} = \Delta P_{contr} + \Delta P_{fr} + \Delta P_{wall} + \Delta P_{\exp}, \quad (4)$$

where ΔP_{contr}, ΔP_{fr}, ΔP_{wall} and $\Delta P_{\exp}$ are contributions from the flow path contraction, channel wall friction, losses through the porous wall and losses due to flow path expansion, respectively, as illustrated in Figure 1.

Although a large number of experimental and modelling studies have been performed to estimate these losses (see [1]-[17] and a review in [8]), they often contradict each other as it is difficult to separate the above contributions. For example, inertial coefficient values can vary in a wide range. Konstandopoulos [4] quotes values between 2.4 and 8.3 obtained by data fitting, while existing theoretical and empirical correlations predict a range around 0.6-0.8 for the typical filter contraction/expansion ratios [3]. As a result, most of the existing modelling work relies on careful calibration of several coefficients.

All of the pressure loss contributions will be inspected here in turn, highlighting the uncertainties and inconsistencies in the existing formulations, and a new model will be suggested to account for the turbulent flow regime.

Through wall losses

The losses through the porous walls are described by the Darcy-Forccheimer equation (e.g. [33]):

$$\Delta P_{porous\ wall} = \frac{\mu}{k} u_w w + \beta \rho u_w^2 w, \quad (5)$$

where u_w is the velocity through wall , w is the wall thickness, μ is the dynamic viscosity, k is wall permeability, ρ is the density and β is the Forchheimer coefficient.

Correct estimate of the wall losses relies heavily on the values of permeability and Forchheimer coefficient. While Forchheimer contribution has been demonstrated to be negligible in multiple studies [3], the linear Darcy losses are very important and increase with filter loading. For example, in Konstandopoulos et al [3] the porous wall losses contribute up to around 70% of the total pressure loss.

Neglecting Forccheimer term and expressing the mean wall velocity using the characteristic inlet channel velocity *U* yields

$$\Delta P_{porous\ wall} = \frac{\mu}{k} \frac{U d_h}{4L} w. \quad (6)$$

The wall permeability can be measured, however availability of appropriate samples and instruments is very limited. Alternatively, it can be estimated from theoretical/empirical expressions (such as Ergun equation [34]) or by fitting expression (5) to the experimental data from wafers (e.g. [13], [16], [35], [36], [37], [38]), filter cores ([13], [14], [39], [40]) or full filter bricks ([4], [15], [41]). None of these methods are very precise, and accuracy has not been thoroughly investigated. Moreover, in testing of filter cores and full filters one needs to consider other losses which are subject to high uncertainty.

It must be noted that the expression (6) is only valid where the wall velocity is uniform. Some authors have looked at including density variation inside the porous wall and inlet/outlet channels ([4]) and compressibility effects ([42], [43]). In our tests the Mach number at the channel entrance can reach values approaching 0.3, however the compressibility effects do not affect the flow considerably, and therefore are not considered here. The density variation, on the other hand, will be much larger for a GPF due to higher pressure drop and temperature gradients, and is important to take into account. Such model modifications come at a cost (more complex formulation, may require numerical solution), and thus are often neglected.

Expansion/contraction losses

Contraction and expansion losses, classified as minor pressure losses, are commonly expressed using the dynamic pressure:

$$\Delta P_{contr} = \zeta_{contr} \frac{\rho U^2}{2}, \quad (7)$$

$$\Delta P_{\exp} = \zeta_{\exp} \frac{\rho U^2}{2}. \quad (8)$$

Here *U* is the velocity in the conduit with smaller cross-section, ρ is gas density and $\zeta_{\exp}$, ζ_{contr} are non-dimensional coefficients called expansion and contraction coefficients, respectively.

The "classical" expressions derived for a single channel contraction/expansion are based on the ratio of the duct cross-section area after the contraction/before expansion (A_1), and the duct cross-section before the contraction/after expansion (A_2):

$$\zeta_{contr} = 0.5\left(1-\frac{A_1}{A_2}\right),\ \zeta_{\exp} = \left(1-\frac{A_1}{A_2}\right)^2 . \quad (9)$$

Other, more accurate expressions exist [44], e.g.:

$$\zeta_{contr} = \left(\frac{1}{c}-1\right)^2 \quad \text{with} \quad c = 0.582 + \frac{0.0418}{1.1-\sqrt{A_1/A_2}} \quad (10)$$

$$\Delta P_{\exp} = \rho U^{1.919}\left(1-\frac{A_1}{A_2}\right)^{1.919} \quad (11)$$

Most of the above correlations have been shown to agree reasonably well with experiments for turbulent flow regime in various configurations (a review of some work is given by Brater in [44]).

Contraction losses for laminar flows are believed to be much higher and are often described using results presented by Kays and London [45]. These have been expressed by Haralampous et al [7] as

$$\zeta_{contr} = 1.1 - 0.4\frac{A_1}{A_2} . \quad (12)$$

However, these results are not very well validated with experimental data for low Reynolds numbers (see Figure 10). Moreover, the supporting experiments have been performed for circular and triangular tube geometries only, while the theoretical expressions vary considerably with the shape of the channels and between single and multiple channel configurations. Some experimental work has been performed more recently on mini- and micro-channels, but results of these are also inconclusive ([46], [47], [48]).

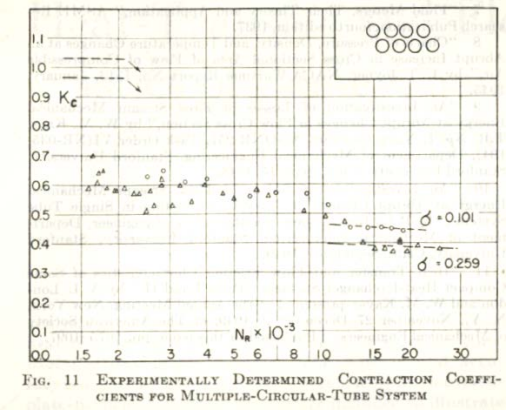

FIG. 11 EXPERIMENTALLY DETERMINED CONTRACTION COEFFICIENTS FOR MULTIPLE-CIRCULAR-TUBE SYSTEM

Figure 10 Contraction coefficients for multiple circular tubes (reproduced from Kays [45]). Symbols correspond to experimental data, broken lines to the appropriate laminar and turbulent flow correlations.

Therefore, it appears that no reliable, validated data exists for laminar contraction losses in square ducts and duct arrays. For the high velocities typical in gasoline applications these losses become more important and ideally would need to be estimated with greater care.

The practical, widely used approach of estimating the contraction/expansion losses in filters relies on using the regression analysis to fit a quadratic to the experimental data, and then using Eq. (5), (7) and (8) to estimate the permeability and the contraction/expansion coefficients [4]. For this purpose, the contraction and expansion coefficients in Eqs. (7) and (8) are combined into one:

$$\Delta P_{contr/\exp} = \zeta_{contr/\exp}\frac{\rho U^2}{2} \quad (13)$$

The resulting values of the combined contraction/expansion coefficient vary in a wide range from < 1 to as high as 8.3 ([3],[4]).

Friction losses

The final contribution from the **friction** in the inlet and outlet channel has been estimated by Konstandopoulos and Johnson [2] as

$$\Delta P_{friction} \approx \frac{2}{3}\frac{\mu F}{d_h^2} UL . \quad (14)$$

In the above, $F = 28.454 = f/Re$ is the correction coefficient for fanning friction factor in a square channel. Expression (14) is equal to 2/3 of the friction loss for a channel with solid walls of the same length with fully developed flow (Hagen-Poiseuille relation). Such losses are consistent with losses in a pipe with side tappings. Massey [49] has estimated friction losses in a pipe with uniform flow through wall tappings as 1/3 of the corresponding loss in a pipe with solid walls. Therefore, for two channels (inlet and outlet) one can double the losses to get the factor of 2/3.

Note that the combination of expressions (6) and (14) is actually an approximation suggested by Konstandopoulos and Johnson [2] to replace their full expression for the pressure loss from friction and through wall losses derived from their 1-dimensional model:

$$\Delta P = \frac{\mu U d_h w}{4Lk}\left\{A_1 + A_2\left[0.5 + \frac{c_1}{g_1}\left(e^{g_1}-1\right) + \frac{c_2}{g_2}\left(e^{g_2}-1\right)\right] + c_1 g_1 + c_2 g_2\right\} \quad (15)$$

where

$$A_1 = \frac{4Lk}{d_h^2 w}Re\ ,\ A_2 = \frac{4L^2 k}{d_h^3 w}F\ ,\ F = 28.454\ , \quad (16)$$

$$g_{1,2} = A_1 \mp \sqrt{A_1^2 + 2A_2}\ ,\ c_{1,2} = \mp 0.5\,\frac{e^{g_{2,1}}+1}{e^{g_2}-e^{g_1}} . \quad (17)$$

In this solution through wall losses and friction losses are fully coupled. Separating these losses into the friction loss represented by Eq. (14) and through wall losses represented by Eq. (6) is only justified for a range of parameters. The authors stated that for the parameters relevant to their study this approximation was valid. However, for the parameters used in this study the approximate solution can deviate from the original solution significantly (Figure 11).

Correlations (14) and (15) have been developed assuming laminar flow and no loss of axial momentum through the porous wall. Presence of slip flow at the porous wall means that the loss of axial momentum through the porous wall may not be negligible, which has been shown in a more recent study [15]. Other assumptions in the above model include constant friction factor $F_1 = 28.454$ for both inlet and outlet channel walls, which again is not strictly speaking true for friction losses in channels with suction/injection and developing flow.

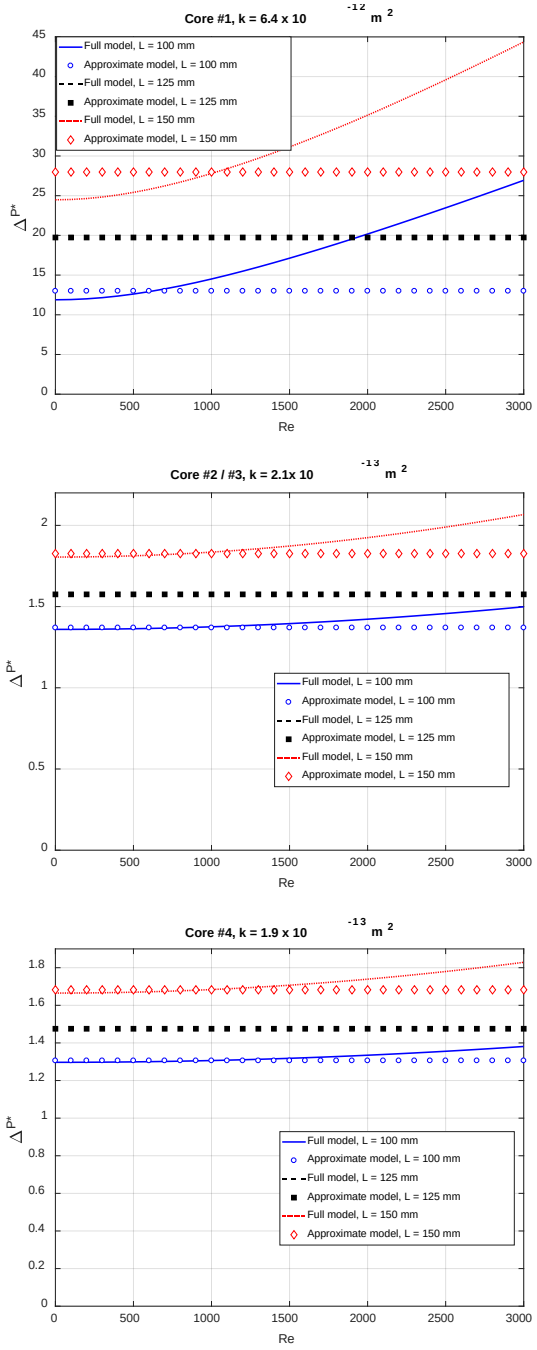

Figure 11 Comparison between non-dimensional pressure loss predicted by full model by Konstandopoulos and Johnson [2] and their approximation, using core parameters from this study and different core lengths. Note that here the non-dimensionalisation from [2] is used for pressure.

Summary

Although the original 1-dimensional model from [2] has been widely used by various authors, most improved models (including the model that takes into account density variation along the channels presented by Konstandopoulos in [4]) are based on the 0-dimensional, decoupled, model from the same study. This is caused by the lack of a closed form solution to the original problem in more complex situations.

The main contributions to the total pressure drop (through wall losses and contraction/expansion losses) depend on accurate determination of two coefficients (wall and soot/ash permeability and contraction/expansion ratio). The widely used approach to using the model introduced in [2] boils down to fitting a quadratic curve to the experimental data, which may result in loss of accuracy when incorrectly estimated friction or through wall losses are masked by artificially inflated contraction/expansion coefficients. In addition, slip effect may play an important role as shown in [16], which adds yet another layer of uncertainty to the model.

Nevertheless, this model and its variations have been successfully used for modelling Diesel Particulate Filters (e.g. [5] - [7]). But even with careful coefficient calibration the model becomes less accurate for high flow rates and temperatures experienced by the Gasoline Particulate Filters.

When the flow becomes turbulent, the wall friction factor is not constant but is a complex function of local flow velocity. This means that the ordinary differential equations describing the flow (equations (1), (2), (6) and (7) in [2]) do not have an analytical solution even in the simplest case and have to be solved numerically. In this work, we look to develop a simple analytical 0-dimensional model based on the 0-dimensional model laminar flow model presented in [2]. It is the first step in attempting to understand and quantify pressure losses in turbulent flow regimes.

0D MODEL REFINEMENT

Friction losses (unplugged cores)

Test results from unplugged (flow-through) cores of different lengths (125 mm and 102 mm) can provide extra information about the friction and contraction/expansion losses in filters. As the air flows through the filter channels, only friction and contraction/expansion losses are present:

$$\Delta P_i = \Delta P_{fr,i} + \Delta P_{contr,i} + \Delta P_{exp,i} \qquad (18)$$

(here i = 5 or 6 is the unplugged core sample number).

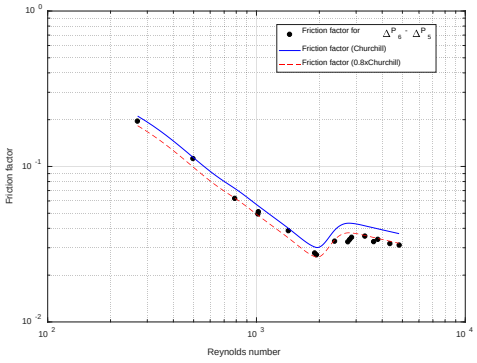

Figure 12 Friction factor calculated for pressure difference between cores #6 and #5

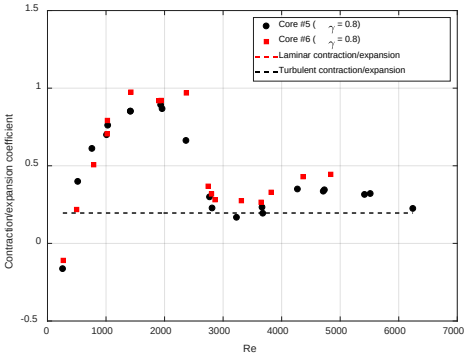

Figure 13 Contraction/expansion coefficient calculated for cores #5 and #6 using Eq. (24) with friction factor shown in Figure 12. The dashed line correspond to correlations (12) and (9) for laminar and turbulent flow regimes, respectively.

As these are cores with the same specification, the contraction/expansion losses for both cores should be approximately the same. Thus, the difference in pressure between the two filters:

$$\Delta P_6 - \Delta P_5 = \Delta P_{fr,6} - \Delta P_{fr,5} \tag{19}$$

is caused mostly by the friction.

Using the Darcy friction factor, *f*, defined from the Darcy-Weisbach equation:

$$\Delta P_{fr} = f \frac{L}{d_h} \frac{\rho U^2}{2} \tag{20}$$

equation (19) can be rewritten as:

$$\Delta P_6 - \Delta P_5 = f \frac{1}{d_h} \frac{\rho U^2}{2} \left(L_6 - L_5 \right) \tag{21}$$

The friction factor determined from Eq. (21) is plotted in Figure 12. Comparison with the friction factor for a channel with solid walls developed by Churchill [50], which covers laminar, transitional and turbulent regimes:

$$f_{Churchill} = 8 \left[\left(\frac{8}{\mathrm{Re}} \right)^{12} + \left(\left[-2.457 \ln \left(\left(\frac{7}{\mathrm{Re}} \right)^{0.9} \right) \right]^{16} + \left[\frac{37530}{\mathrm{Re}} \right]^{16} \right)^{-1.5} \right]^{1/12} \tag{22}$$

shows a very good qualitative agreement. A clear transition from laminar to turbulent flow is evident for Reynolds numbers between 2000 and 4000.

As discussed before, friction factors in porous channels can differ significantly from those in a channel with smooth or rough walls, and presence of porous walls can delay/promote early transition. It appears that the cold flow in the filters considered has transition characteristics consistent with a channel with smooth walls. The offset between the theoretical friction factor and the experimental data in Figure 12 may be explained by the presence of porous walls and associated wall slip effect where the wall velocity is not zero. Further investigation would be beneficial, however for this study we use the full friction factor as described by Eq. (22) which results in a good agreement with the experimental data (Figure 14).

Friction losses (plugged cores)

Without further investigation, it is difficult to determine whether the flow in plugged cores is fully laminar, fully turbulent, transitional or all of these regimes in different sections of the channels. However, a clear indication of the flow transition can be seen in the test results for plugged cores (Figure 6 (a)). Two trend lines with slopes consistent with laminar fully developed flow (Re^{-1}) and turbulent fully developed flow ($Re^{-0.25}$) are shown, and the data follow these trends for Reynolds numbers below and above $Re \sim 3000$, respectively. If the friction losses remained laminar (i.e. proportional to velocity), then the inertial losses would dominate at high mass flow rates with the non-dimensional pressure becoming nearly constant. This is clearly not the case.

Assuming that transition indeed occurs and is controlled by the value of the Reynolds number at the entrance into the inlet channel, a simple analogy can be used to extend the existing model described in [2] from laminar flow regime to turbulent. As the laminar flow losses in inlet/outlet channel have been shown to be roughly equivalent to 2/3 of the corresponding losses in a channel with solid walls and fully developed flow, we estimate the pressure loss due to friction in turbulent flow as 2/3 of the losses expressed by Eq. (20):

$$\Delta P_{friction,turbulent} = \frac{2}{3} f \frac{\rho U^2}{2} \frac{L}{d_h} \tag{23}$$

with the friction factor (22) covering laminar, turbulent and transitional flow regimes. As discussed before, flow in a channel with porous walls can be argued to be a limiting case of flows in pipes with side tappings, for which the pressure losses have been shown to be 2/3 of the corresponding losses in a channel with no mass sinks [49]. This provides extra justification for using this factor, although further studies would be needed to represent this term better.

Contraction/expansion losses

The unplugged core data has been further used for a rough estimate of the contraction/expansion losses. Assuming that the friction coefficient is known, the inertial losses can be expressed as

$$\Delta P_{contr/\exp} = \zeta_{contr/\exp} \frac{\rho U^2}{2} = \Delta P_{total} - \Delta P_{fr} .$$

Then contraction/expansion coefficient can be calculated using expression

$$\zeta_{\exp/contr} = \left[\Delta P_{total} - \Delta P_{fr} \right] \Big/ \left[\frac{\rho U^2}{2} \right] . \tag{24}$$

The resulting values of contraction/expansion coefficients are shown in Figure 13. The results are sensitive to the value of the friction correction factor, however even lower values the contraction/expansion coefficient is of the same order as predicted by the existing expressions for both laminar and turbulent range. Other factors may affect the values of calculated coefficients such as flow losses due to the boundary layer development in the laminar regime.

In absence of more accurate data for the contraction/expansion coefficients, expressions (9) are used here.

Through wall losses

As mentioned before, different methods of testing permeability are likely to produce different values. Moreover, permeability of the walls of catalyst-coated filters will vary considerably in different parts of the filter because of high variability of the coating parameters [16]. A preliminary investigation of uncoated filters used in this study has been performed in [16] with a resulting mean value of $k_{wafer} = 6.4\times10^{-12}$ (m^2) based on 7 wafer samples. This value will be used to illustrate the performance of the model presented here for core #1. A slip correction is applied for Core #1 so that

$$k = k_{wafer}\left(1 + C\frac{P_{down}}{P_{up}}\mu\sqrt{T}\right) \tag{25}$$

with slip correction coefficient C = 806.4, as derived for bare wafers in [16]. Note that the pressure ratio factor has been introduced to account for permeability variation with pressure [51]. For other cores, a fitting procedure has been used as described below. Slip properties of the coated walls are not known and therefore are not used here.

SUGGESTED TURBULENT FLOW MODEL

Here we demonstrate how the turbulent friction losses can be incorporated by expanding the model widely used in literature [2]. The model combines losses described by Eq. (4) with expressions (13), (20) and (6):

$$\Delta P = \zeta_{contr/\exp}\frac{\rho U^2}{2} + \frac{2}{3}f\frac{L}{d_h}\frac{\rho U^2}{2} + \frac{\mu}{k}\frac{Ud_h}{4L}w\,. \tag{26}$$

For simplicity, here the density and velocity upstream of the core are used. Since these depend on the temperature and upstream pressure, we need to rearrange expression (26) to eliminate upstream pressure on the right-hand side. Using

$$j_m = U\rho_{up}\,,\quad \rho_{up} = \frac{P_{up}}{RT}\,, \tag{27}$$

where $j_m = \frac{\dot{m}_{channel}}{A_{channel}}$ is mass flux, $\dot{m}_{channel}$ is mass flow through one channel, $A_{channel}$ is one channel cross-section area, P_{up} is upstream pressure and T is upstream temperature, we can rearrange (26) as

$$\Delta P = \frac{j_m RT}{P_{up}}\left[\zeta_{contr/\exp}\frac{j_m}{2} + \frac{2}{3}f\frac{L}{d_h}\frac{j_m}{2} + \frac{\mu d_h w}{4kL}\right] \tag{28}$$

or

$$P_{up} - P_{down} = \frac{j_m RT}{P_{up}}\left[\zeta_{contr/\exp}\frac{j_m}{2} + \frac{2}{3}f\frac{L}{d_h}\frac{j_m}{2} + \frac{\mu d_h w}{4kL}\right] \tag{29}$$

where P_{down} is the downstream pressure. Downstream pressure can usually be estimated, and is equal to atmospheric pressure in the testing presented here. Then upstream pressure can be expressed from Eq. (29):

$$P_{up} = 0.5\left(P_{down} + \sqrt{P_{down}^2 + 4j_m RT\left[\zeta_{contr/\exp}\frac{j_m}{2} + \frac{2}{3}f\frac{L}{d_h}\frac{j_m}{2} + \frac{\mu d_h w}{4kL}\right]}\right) \tag{30}$$

Equation (30) is a simple 0-dimensional model describing pressure losses in a filter. All contributions to pressure loss are estimated from known empirical and analytical expressions, and only one parameter (porous wall permeability) is required. The permeability can be estimated by rearranging Eq (26):

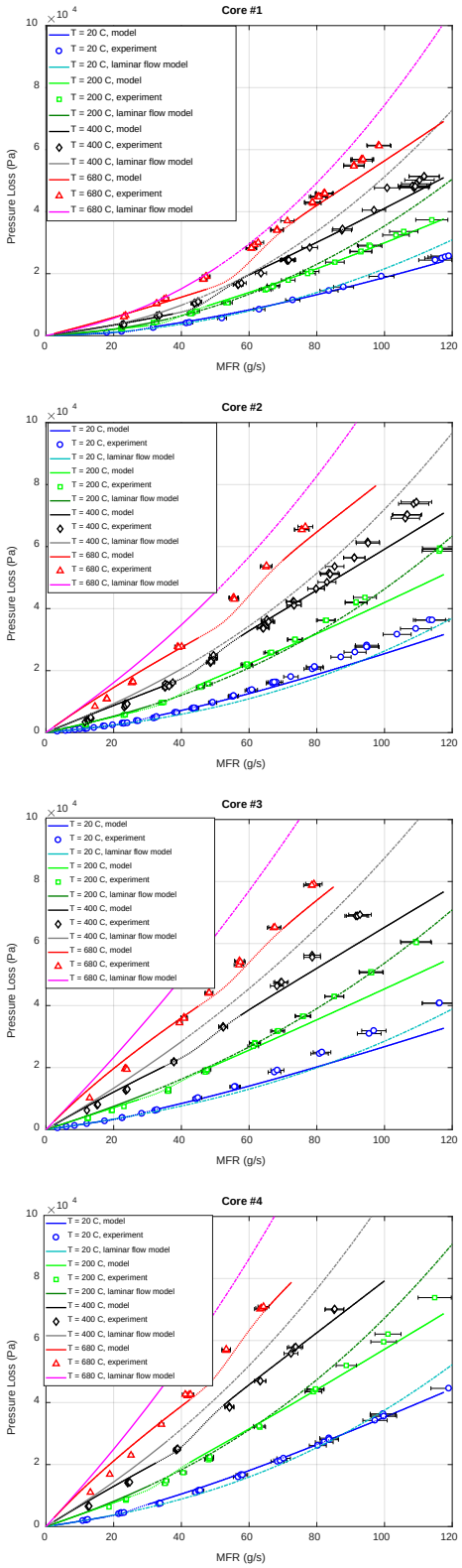

Figure 14 Comparison of the improved model with experiments. Dotted part of the lines indicates transition regime (Reynolds number between 2000 and 3000). Dash-dot lines indicate laminar model predictions in the turbulent Reynolds number range.

$$\Delta P - \zeta_{contr/\exp}\frac{\rho U^2}{2} - \frac{2}{3} f \frac{L}{d_h}\frac{\rho U^2}{2} = \frac{\mu}{k}\frac{U d_h}{4L} w = D \times U \ .$$

and using linear regression to estimate coefficient D. Then the permeability is equal to

$$k = \frac{\mu d_h w}{4LD} \ .$$

Since the inertial losses are estimated roughly from the correlations derived for single ducts, any errors will grow with the square of velocity. In addition, transition regime is not expected to be predicted well. Therefore, only laminar flow regime test results are used here for estimation of the wall permeability. The resulting values for cores #2, #3 and #4 are $k = 1.9 \times 10^{-13}$ (m^2), $k = 1.3 \times 10^{-13}$ (m^2) and $k = 1.7 \times 10^{-13}$ (m^2), respectively. Note that two different permeability values have been obtained for cores #2 and #3, which have "identical" wall structure. This is the result of the uneven coating often present in coated filter substrates (as discussed in [16]) caused by the coating procedure where inlet and outlet channels are coated separately, and the different depth of coating penetration into the bare filter walls in different filter sections.

Comparison with experimental results (Figure 14) shows a good agreement for most cores in most regimes. The transition losses (dotted parts of the model prediction lines) are not predicted well, which is hardly surprising given the complex properties of the flow. Model also underpredicts losses for the shorter core. This can be attributed to the fact that the wall velocity distribution along the channel is very different for a shorter core, while the model assumes uniform wall flow along the channels.

The effect of slip at high mass flow rates is insignificant. If the slip correction is not included, the total pressure loss predicted by the model changes by less than 2% in the whole turbulent flow range for all temperatures for all cores.

In order to compare the performance of the suggested model with the model based on Bisset [1] and developed in [2], the laminar flow model described by Eqs. (15) and (13) is shown in Figure 14 with the inertial coefficients described by Eqs. (9) and the permeability values shown above. The laminar flow model fits the data reasonably well for low Reynolds numbers for cold flow (solid lines). The dash-dotted lines show laminar model predictions for Reynolds numbers above 2000. Although laminar flow model has been used by other authors outside the laminar flow range (e.g. in [4] and [15] the maximum Reynolds number considered is greater than 2000), Figure 14 clearly shows that it fails to describe pressure loss trends for the whole parameter range. Note that for high flow rates predictions by both models are affected by considerable density variation along the channel cause by the high pressure gradients. The original laminar flow model [2] was based on an assumption of constant density along the channel, and this is how it is used here. Although there have been attempts to account for density variation along the channel [4], these are usually not based on the full model described by Eq. (15) and thus are less accurate even in the laminar flow regime.

In summary, the existing models can be calibrated to fit the experimental data, but the resulting parameter values are not representative of the flow physics and therefore are likely to fail to correctly predict pressure loss in conditions different to the range used for calibration. In contrast, the model suggested here is based on solid fluid dynamics principles.

This model is the first attempt to incorporate turbulent flow losses into the 0-dimensional model, and is based on multiple assumptions, such as:

- The flow transition in both channels follows similar pattern to the transition in channels with solid walls
- Reynolds number at the entrance of the inlet channel, based on mean velocity and channel diameter, determines the transition point
- Uniform wall velocity is assumed along the channel (which results in the factor of 2/3 in friction loss estimation)
- Constant density (equal to upstream value) is used for velocity and other parameter estimation in both channels
- Constant temperature distribution is assumed
- Contraction and expansion factors are assumed to be equal to the expressions used for minor losses in turbulent flows, derived for a single circular pipe
- There is no axial momentum transfer at the porous wall surface
- The flow upstream of the test section is uniform.

Note that although the model is essentially 0-dimensional, it can be used for three-dimensional modelling of aftertreatment systems using the porous medium approach widely adopted for catalytic converters, where the pressure loss along the flow path is calculated from the local flow velocity value at the entry into the catalyst channel [52].

CONCLUSIONS

This paper highlights the need for improvement of the widely used one-dimensional pressure loss model for particulate filters. Using experimental measurements of pressure losses in unplugged and plugged filter cores, the flow regime change from laminar to turbulent has been demonstrated. Although the friction coefficients obtained from experiments are lower than the theoretical predictions, the results clearly demonstrated that properties of flow transition in porous filter channels are very similar to those of channels with solid walls and occur at the same range of channel Reynolds numbers. These experiments also allowed to estimate the inertial losses associated with flow path contraction and expansion. It appears that in many existing studies these high flow losses could have been masked by inflated inertial coefficients with values much higher than those published for single and multiple channels in laminar and turbulent flows.

A simple model incorporating an estimate of turbulent flow friction losses from Colebrook equation solution and textbook expressions for inertial losses due to flow path contraction and expansion is suggested, and is shown to perform well for a wide range of mass flows and temperatures. This model requires only one calibration parameter, namely porous wall permeability. Slip effect can also be included, which requires an extra parameter (slip coefficient), but its contribution is small (< 2%) in the turbulent flow regime and therefore can be neglected.

The proposed model is based on several assumptions, some of which (for example, assuming the same flow regime in the whole domain based on the inlet Reynolds number) may limit the accuracy of the results. On the other hand, this allows to have a closed form analytical solution for estimation of the pressure losses, which is important for initial design considerations.

The model can be considerably improved by accounting for density variation along the channel, velocity variation along the channel, refinement of the inertial loss coefficient values (especially for laminar flow regime where these are largely unknown) and slip flow correction [16]. This is the subject of future work.

REFERENCES

[1] Bissett, E.J., "Mathematical Model of the Thermal Regeneration of a wall-flow monolith diesel particulate filter," Chemical Engineering Science 39: 1233-1244, 1984, doi:10.1016/0009-2509(84)85084-8

[2] Konstandopoulos, A.G. and Johnson, H., "Wall-Flow Diesel Particulate Filters - Their Pressure Drops and Collection Efficiency," SAE Technical Paper 890405, 1989, doi:10.4271/890405

[3] Konstandopoulos, A.G., Skaperdas, E. and Masoudi, M., "Inertial Contributions to the Pressure Drop of Diesel Particulate Filters," SAE Technical Paper 2001-01-0909, 2001, doi:10.4271/2001-01-0909

[4] Konstandopoulos A.G.,"Flow Resistance Descriptors for Diesel Particulate Filters: Definitions, Measurements and Testing," SAE Technical Paper 2003-01-0846, 2003, doi:10.4271/2003-01-0846

[5] Masoudi, M., Heible, A. and Then, P.M., "Predicting Pressure Drop of Wall-Flow Diesel Particulate filters - theory and experiment," SAE Technical Paper 2000-01-0184, 2000, doi:10.4271/2000-01-0184

[6] Masoudi, M., Konstandopoulos A.G., Nikitidis, M.S., Skaperdas, E., Zarvalis, D., Kladopoulu E. and Altiparmakis, C., "Validation of a Model and Development of a Simulator for Predicting the Pressure Drop of Diesel Particulate Filters," SAE Technical Paper 2001-01-0911, 2001, doi:10.4271/2001-01-0911

[7] Haralampous, G.A., Kandylas, I. P., Koltsakis, G.S. and Samaras, Z.C., "Diesel particulate filter pressure drop. Part 1: modelling and experimental validation," International Journal of Engine Research 5(2): 149-162, 2004, doi: 10.1243/146808704773564550

[8] Koltsakis, G., Haralampous, O., Depcik, C. and Ragone, J.C., "Catalyzed diesel particulate filter modeling," Reviews in Chemical Engineering 29(1): 1-61, 2013, doi:10.1515/revce-2012-0008

[9] Yang, S., Deng, C., Gao, Y. and He, Y., "Diesel particulate filter design simulation: A review" Adv. Mech. Eng. 8(3):1-14, 2016, doi:10.1177/1687814016637328

[10] Opris, C.N. and Johnson, J.H., "A 2-D computational model describing the flow and filtration characteristics of a ceramic Diesel Particulate Trap," SAE technical Paper 980545, 1998, doi:10.4271/980545

[11] Oxarango, L., Schmitz, P. and Quintard, M., "Laminar flow in channels with wall suction or injection: a new model to study multi-channel filtration systems," Chemical Engineering Science 59:1039-1051, 2004, doi:10.1016/j.ces.2003.10.027

[12] Piscaglia F., Rutland, C.J. and Foster, D.E. " Development of a CFD Model to Study the Hydrodynamic Characteristics and the Soot Deposition Mechanism on the Porous Wall of a Diesel Particulate Filter," SAE Technical Paper 2005-01-0963, doi:10.4271/2005-01-0963

[13] Lambert, C., Chanko, T., Dobson, D. and Pakko, J., "Gasoline Particle Filter Development," Emissions Control Science and Technology 3: 105-111, 2017, doi:10.1007/s40825-016-0055-x

[14] Lambert, C., Bumbaroska, M., Dobson, D., Hangas, J., Pakko, J. and Tenison, P., "Analysis of High Mileage Gasoline Exhaust Particle Filters," SAE Technical Paper 2016-01-0941, doi:10.4271/2016-01-0941

[15] Watling, T.C., Ravenscroft, M.R., Cleeton, J.P.E., Rees, I.D. and Wilkins, D.A.R., "Development of a Particulate Filter Model for the Prediction of Backpressure: Improved Momentum Balance and Entrance and Exit Effect Equations," SAE Technical Paper 2017-01-0974, 2017, doi:10.4271/2017-01-0974

[16] Aleksandrova, S., Saul, J., Medina, H., Garcia-Afonso, O., Lin, C., Herreros, J.M., Bevan, M. and Benjamin, S.F., "Gasoline Particulate Filter wall permeability testing", SAE Int. J. Engines 11(5):2018

[17] Masoudi, M., "Hydrodynamics of Diesel Particulate Filters," SAE Technical Paper 2002-01-1016, 2002, doi:10.4271/2002-01-1016

[18] York, A., Watling, T., Ramskill, N., Gladden, L. et al., "Visualization of the Gas Flow Field within a Diesel Particulate Filter Using Magnetic Resonance Imaging," SAE Technical Paper 2015-01-2009, 2015, https://doi.org/10.4271/2015-01-2009

[19] Suga, K. and Nishio, Y., "Three-dimensional macroscopic flow simulation across the interface of a porous wall and clear fluid by the Lattice Boltzmann Method," The Open Transport Phenomena Journal 1:35-44, 2009

[20] Breugem, W.P., Boersma, B.J. and Uittenbogaard, R.E., "The influence of wall permeability on turbulent channel flow," J. Fluid Mech. 562:35-72, 2006

[21] Rosti, M.E., Cortelezzi, L. and Quadrio, M., "Direct numerical simulation of turbulent channel flow over porous walls," J. Fluid Mech. 784:396-442, 2015

[22] Breugem, W.P. and Boersma, B.J., "The turbulent flow over a permeable wall," Proceedings of the summer program 2002, Center for Turbulence Research, Stanford University, US, 2002

[23] Eckert, E.R.G., Donoughe, P.L., and Moore, B. J., "Velocity and Friction characteristics of laminar viscous boundary-layer and channel flow over surfaces with ejection or suction," National Advisory Committee for Aeronautics, Technical Note 4102, 1957

[24] Raithby, G., "Laminar heat transfer in the thermal entrance region of circular tubes and two-dimensional rectangular ducts with wall suction and injection," Int. Journal of Heat and Mass Transfer 14(2):223-243, 1971, doi: 10.1016/0017-9310(71)90091-3

[25] Wang, J., Gao, Z., Gan, G. and Wu, D., "Analytical solution of flow coefficients for a uniformly distributed porous channel," Chemical Engineering Journal 84:1- 6, 2001

[26] Hassanzadeh, H., and Mehrabian, M.A., "Modelling heat and mass transfer in laminar forced flow between parallel plates with suction or injection boundary conditions," Iranian J. of Hydrogen & Fuel Cell 1:35-46, 2015

[27] Schlatter, P., and Orlu, R., "Turbulent asymptotic suction boundary layers studied by simulation," Journal of Physics: Conference Series 318:022020, 2011

[28] Oyewola, O., Djenidi, L., and Antonia, R.A., "Effect of wall suction on a turbulent boundary layer: Reynolds number dependence," 14th Australian Fluid Mechanics Conference, Adelaide, Australia, 2001

[29] Bellettere, J., Bataille, F. and Lallemand A., "A new approach for the study of turbulent boundary layers with blowing," Int. J. Heat and Mass Transfer 42:2905-2920, 1999

[30] Schildknecht, M., Miller, J.A., and Meier, G.E.A., "The influcence of suction on the structure of turbulence in fully developed pipe flow," J Fluid Mech 90(1):67-107 (1979)

[31] Moussy, Y., and Snider, A.D., "Flow within a pipe annulus with injection and suction through a porous wall with high wall Reynolds numbers," Transactions of ASME: Journal of Fluids Engineering 133:014501-1 - 014501-5 (2011)

[32] Tilton, N., and Cortelezzi, L., "Stability of Boundary Layers over porous walls with suction," AIAA Journal 53(10):2856-2868 (2015)

[33] Konstandopoulos, A.G., Skaperdas, E., Warren, J. and Allansson, R., "Optimized filter design and selection criteria for continuously regenerating diesel particulate traps," SAE Technical Paper 1999-01-0468, doi:10.4271/1999-01-0468

[34] Ergun, S., “Fluid Flow through Packed Columns,” Journal of Chemical Engineering Progress, 48(2):89-94, 1952

[35] Wirojsakunchai, E., Kolodziej, C., Yapaulo, R., and Foster, D., "Development of the Diesel Exhaust Filtration Analysis System (DEFA)," SAE Int. J. Fuels Lubr.1(1): 265-273, 2009, 10.4271/2008-01-0486

[36] Martirosyan, K.S., Chen, K. and Luss, D., " Behavior features of soot combustion in diesel particulate filter," Chemical Engineering Science 65:42-46, 2010, doi:10.1016/j.ces.2009.01.058

[37] Viswanathan, S., Rothamer, D., Zelenyuk, A., Stewart, M. and Bell, D., "Experimental investigation of the effect of inlet particle properties on the capture efficiency in an exhaust particulate filter," Journal of Aerosol Science 113:250-264, 2017, doi:10.1016/j.jaerosci.2017.08.002

[38] Kamp, C.J., Zhang, S., Bagi, S., Wong, V., Monahan, G., Sappok, A. and Wang, Y., "Ash Permeability Determination in the Diesel Particulate Filter from Ultra-High Resolution 3D X-Ray Imaging and Image-Based Direct Numerical Simulations," SAE Int. J. Fuels Lubr. 10(2):608-618, 2017, doi:10.4271/2017-01-0927.

[39] Liu, X., Kim, J., Chanko, T., Lambert, C. et al., "A Modeling Analysis of Fibrous Media for Gasoline Particulate Filters," SAE Technical Paper 2017-01-0967, 2017, doi:10.4271/2017-01-0967

[40] Versaevel, P., Colas, H., Rigaudeau, C., Noirot, R. et al., "Some Empirical Observations on Diesel Particulate Filter Modeling and Comparison Between Simulations and Experiments," SAE Technical Paper 2000-01-0477, 2000, https://doi.org/10.4271/2000-01-0477

[41] Konstandopoulos, A., Kostoglou, M., Skaperdas, E., Papaioannou, E. et al., "Fundamental Studies of Diesel Particulate Filters: Transient Loading, Regeneration and Aging," SAE Technical Paper 2000-01-1016, 2000, https://doi.org/10.4271/2000-01-1016

[42] Depcik, C., Langness, C., and Mattson, J., "Development of a Simplified Diesel Particulate Filter Model Intended for an Engine Control Unit," SAE Technical Paper 2014-01-1559, 2014, doi:10.4271/2014-01-1559

[43] Cunningham, P. and Meckl, P., "1-D Dynamic Diesel Particulate Filter Model for Unsteady Pulsating Flow," SAE Technical Paper 2007-01-1140, 2007, https://doi.org/10.4271/2007-01-1140

[44] Brater, E.F., King, H.W., Lindell, J.E. and Wei, C.Y, "Handbook of hydraulics, Seventh Edition," (McGraw-Hill, 1996), 6.32-6.37, ISBN 0-07-007247-7

[45] Kays, W.M., "Loss Coefficient for Abrupt Changes in Flow Cross Section with Reynolds Number Flow in Single and Multiple Mube Systems," Transactions of the American Society of Mechanical Engineers, 72:1067-1074, 1950

[46] Yu, J., Li, Z., and Ma, C.F., "Experimental study of pressure loss due to abrupt expansion and contraction in mini-channels," Proceedings of the 13th International Heat Transfer Conference, Sydney, Begell House (2006)

[47] Chalfi, T.Y., and Ghiaasiaan, S.M., "Pressure drop caused by flow area changes in capillaries under low flow conditions," International Journal of Multiphase Flow 34:2-12 (2008)

[48] Guo, H., Wang, L., Yu, J., Ye, F. Ma, C., and Li, Z., "Local resistance of fluid flow across sudden contraction in small channels," Front. Energy Power Eng. China 4(2):149–154 (2010) doi:10.1007/s11708-009-0060-7

[49] Massey, B.S., "Mechanics of Fluids, Sixth edition," (Van Nostrand Reinhold (International), 1989), 225, ISBN 0-278-00047-9

[50] Churchill, S.W., "Friction-factor equation spans all fluid flow regimes," Chemical Engineering 84:91–102, 1977

[51] Pulkrabek, W.W., and Ibele, W.E., "The effect of temperature on the permeability of a porous material," Int. J. Heat Mass Transfer 30:1103-1109 (1987)

[52] Benjamin, S.F. and Roberts, C.A., "Methodology for modelling a combined DPF and SCR catalyst with the porous medium approach in CFD," SAE International Journal of Engines 7(4):1997-2011, 2014, doi:10.4271/2014-01-2819.

NOMENCLATURE

A_0	m^2	Cross-section area of the test section
A_1	m^2	Cross-section area of a channel downstream of the contraction or upstream of the expansion
A_2	m^2	Cross-section area of a channel upstream of the contraction or downstream of the expansion
a	m	Filter cell pitch calculated as $0.0254 / \sqrt{cells\ per\ square\ inch}$
c	-	the ratio of areas of the vena contracta and the outlet pipe
D	Pa s / m	Linear regression coefficient
d_h	m	Hydraulic diameter of a filter inlet/outlet channel
$F = 28.454 = f/Re$	-	Correction coefficient for fanning friction factor in a square channel
f	-	Fanning friction factor
$f' = \gamma f$	-	Fanning friction factor with correction for filter wall properties
j_m	$kg/s/m^2$	Mass flux at the entrance to the inlet channel
k	m^2	Filter wall permeability
L	m	Filter length
$\dot{m}$	kg/s	Mass flow rate at the entrance of the inlet filter channel
P_{down}	Pa	Pressure downstream of the filter outlet channel
P_{up}	Pa	Pressure upstream of the filter inlet channel
R	J/(kg K)	Gas constant
$Re = \frac{Ud_h}{\nu}$	-	Reynolds number

T	K	Temperature upstream of the filter inlet channel
U	m/s	Mean velocity at the entrance to the filter inlet channel
w	m	Filter wall thickness
ΔP	Pa	Pressure loss
$\Delta P^* = \frac{\Delta P}{0.5\rho U^2}$	-	Non-dimensional total pressure loss
ΔP_{contr}	Pa	Pressure loss due to flow path contraction into the inlet channel
$\Delta P_{\exp}$	Pa	Pressure loss due to flow path expansion from outlet channel
ΔP_{fr}	Pa	Pressure loss due to wall friction inside the inlet and outlet channels
ΔP_{total}	Pa	Total pressure loss across a particulate filter
ΔP_{wall}	Pa	Pressure loss through the porous filter wall
γ	-	Friction correction factor to account for filter wall properties
μ	kg/(m s)	Dynamic viscosity
ν	m^2/s	Kinematic viscosity
ρ	kg/m^3	Density
ρ_{up}	kg/m^3	Density upstream of the filter inlet channel
σ	-	Open area fraction at the front face of the filter core
ζ_{contr}	-	Contraction coefficient
$\zeta_{contr/\exp} = \zeta_{contr} + \zeta_{\exp}$	-	Combined contraction/expansion coefficient
$\zeta_{\exp}$	-	Expansion coefficient

DEFINITIONS/ABBREVIATIONS

DPF	Diesel Particulate Filter
GPF	Gasoline Particulate Filter
MFR	Mass Flow Rate
SCF	Stokes-Cunnigham Factor
SCRF	Selective Catalytic Reduction Filter
TMAC	Tangential Momentum Accommodation Coefficient
VFM	Viscous Flow Meter